ChemPubSoc Europe

DOI: 10.1002/cssc.201900534

CHEMSUSCHEM Full Papers

Scaling-Up of Bio-Oil Upgrading during Biomass Pyrolysis over ZrO_2/ZSM-5-Attapulgite

Héctor Hernando,[a, b] Ana M. Hernández-Giménez,[c] Santiago Gutiérrez-Rubio,[a] Tomaz Fakin,[d] Andrej Horvat,[d] Rosa M. Danisi,[e] Patricia Pizarro,[a, b] Javier Fermoso,[a] Eleni Heracleous,[f] Pieter C. A. Bruijnincx,[c] Angelos A. Lappas,[f] Bert M. Weckhuysen,[c] and David P. Serrano*[a, b]

Ex situ catalytic biomass pyrolysis was investigated at both laboratory and bench scale by using a zeolite ZSM-5-based catalyst for selectively upgrading the bio-oil vapors. The catalyst consisted of nanocrystalline ZSM-5, modified by incorporation of ZrO_2 and agglomerated with attapulgite (ZrO_2/n-ZSM-5-ATP). Characterization of this material by means of different techniques, including CO_2 and NH_3 temperature-programmed desorption (TPD), NMR spectroscopy, UV/Vis microspectroscopy, and fluorescence microscopy, showed that it possessed the right combination of accessibility and acid–base properties for promoting the conversion of the bulky molecules formed by lignocellulose pyrolysis and their subsequent deoxygenation to upgraded liquid organic fractions (bio-oil). The results obtained at the laboratory scale by varying the catalyst-to-biomass ratio (C/B) indicated that the ZrO_2/n-ZSM-5-ATP catalyst was more efficient for bio-oil deoxygenation than the parent zeolite n-ZSM-5, producing upgraded bio-oils with better combinations of mass and energy yields with respect to the oxygen content. The excellent performance of the ZrO_2/n-ZSM-5-ATP system was confirmed by working with a continuous bench-scale plant. The scale-up of the process, even with different raw biomasses as the feedstock, reaction conditions, and operation modes, was in line with the laboratory-scale results, leading to deoxygenation degrees of approximately 60% with energy yields of approximately 70% with respect to those of the thermal bio-oil.

Introduction

Biomass pyrolysis has attracted much interest for the production of liquid biofuels, mainly by using lignocellulosic residues as the raw material.[1] It is a relatively simple process that takes place in a non-oxidative medium at atmospheric pressure. The optimum conditions for maximizing the yield of the liquid fraction (bio-oil) comprise intermediate temperatures, typically in the range 500–600 °C, and high heating rates (fast pyrolysis).[2,3] The bio-oil so obtained contains high amounts of oxygen and water, and has a low heating value, acidic pH, and low stability.[4]

Bio-oil upgrading has been investigated by a variety of physical and chemical methods. Chemical transformations applied to the bio-oil include catalytic pyrolysis, hydrodeoxygenation, ketonization, aldol condensation, esterification, and alkylation.[2,5–9] In most cases, these transformations are aimed to reduce (at least partially) the oxygen content of the bio-oil, thus bringing its chemical composition closer to that typical of fossil-derived fuels. Catalytic pyrolysis presents the advantage of operating at atmospheric pressure and can thus be easily combined with the biomass thermal step.[10] This can be accomplished by adding the catalyst directly to the pyrolysis reactor (in situ system) or by connecting the catalyst bed in series with the pyrolysis zone (ex situ system).[3,4,11] In the latter scheme, it is possible to operate the thermal and catalytic

[a] H. Hernando, S. Gutiérrez-Rubio, Dr. P. Pizarro, Dr. J. Fermoso, Prof. D. P. Serrano
Thermochemical Processes Unit
IMDEA Energy Institute
28935, Móstoles, Madrid (Spain)
E-mail: david.serrano@imdea.org

[b] H. Hernando, Dr. P. Pizarro, Prof. D. P. Serrano
Chemical and Environmental Engineering Group, ESCET
Rey Juan Carlos University
28933, Móstoles, Madrid (Spain)

[c] Dr. A. M. Hernández-Giménez, Prof. P. C. A. Bruijnincx, Prof. B. M. Weckhuysen
Inorganic Chemistry and Catalysis group
Debye Institute for Nanomaterials Science
Utrecht University
Universiteitsweg 99, 3584 CG Utrecht (The Netherlands)

[d] T. Fakin, A. Horvat
SILKEM, d.o.o.
Tovarniška cesta 10, SI-2325 Kidričevo (Slovenia)

[e] Dr. R. M. Danisi
Institute of Applied Geosciences–Technical Petrophysics
Karlsruhe Institute of Technology
Adenauerring 20b, 76131 Karlsruhe (Germany)

[f] Dr. E. Heracleous, Prof. A. A. Lappas
Chemical Process and Energy Resource Institute (CPERI)
Centre for Research and Technology Hellas (CERTH)
57001, Thermi, Thessaloniki (Greece)

Supporting Information and the ORCID identification number(s) for the author(s) of this article can be found under: https://doi.org/10.1002/cssc.201900534.

steps at different temperatures and avoid direct contact between the biomass and the catalyst. The solid fraction (char) produced by thermal biomass pyrolysis is accumulated in the thermal zone in the ex situ configuration, which is not in contact with the catalyst; a fact that helps in attenuating catalyst deactivation.[3,10]

A large number of solid catalysts have been tested in biomass catalytic pyrolysis, including zeolites,[12,13] amorphous silica–alumina,[14,15] ordered mesoporous materials,[16,17] and metal oxides.[18–21] Most of the works have been focused on the use of zeolites owing to their excellent performance in catalytic cracking reactions. In particular, zeolite ZSM-5 has shown remarkable properties for biomass catalytic pyrolysis, leading to the formation of upgraded bio-oils with a high concentration of aromatic hydrocarbons.[22–25] However, zeolitic catalysts suffer from fast deactivation by the deposition of carbonaceous residues, whereas the yield finally obtained for the upgraded bio-oil is often very low owing to the extensive formation of gases and coke.[4] Accordingly, much research effort has been recently devoted to tuning the properties of zeolite-based catalysts to improve their accessibility, suppress secondary reactions, and decrease the coke deposition. Thus, zeolite ZSM-5 has been modified by reducing its crystal size, introducing secondary porosity, and incorporating a variety of metals and metal-oxide phases.[10,26–34] Most studies in the literature have been performed at laboratory scale by using catalysts in powder form. Investigation of the scale-up of the process with the use of technical catalysts has been scarcely covered.

In a recent work, we demonstrated the remarkable and positive effect of modifying zeolite ZSM-5 in nanocrystalline form by impregnation of ZrO_2 over the external surface of the zeolite nanocrystals because this moderates and complements the zeolite acidity.[35] We showed in a further work that the use of clay binders for the agglomeration of pyrolysis catalysts also has a noticeable influence on their behavior in biomass catalytic pyrolysis. In particular, the use of attapulgite (ATP) as a binder enabled the production of upgraded bio-oil with enhanced yield and low oxygen content.[36] Within this context, the current work reports the excellent performance of the ZrO_2/n-ZSM-5-ATP catalyst material for the production of bio-oil with improved properties by lignocellulose pyrolysis for reaction systems operating at different scales and operation modes (i.e., batch and continuous). Moreover, the effect of the catalyst-to-biomass (C/B) ratio is assessed, providing valuable information on the main reaction pathways occurring during bio-oil upgrading over this catalyst.

Results and Discussion

Catalyst properties

The main physicochemical properties of the technical ZrO_2/n-ZSM-5-ATP catalyst, the pure zeolite, and the impregnated ZrO_2/n-ZSM-5 are summarized in Table 1. The influence of using attapulgite as the binder was analyzed in depth in our previous work.[36] Synergetic effects between the zeolite and the clay were found to occur in the technical ZrO_2/n-ZSM-5-ATP catalyst, affecting both the acidic and basic features of the material. The quantity of ZrO_2 incorporated into the zeolitic support, determined by inductively coupled plasma optical emission spectroscopy (ICP-OES), matches well with the theoretical value (10 wt%). A reduction in the textural properties was observed after agglomeration of the parent ZrO_2/n-ZSM-5 material with attapulgite, which is a direct consequence of the lower surface area of the pure clay (107 $m^2 g^{-1}$). In this way, the decrease of the micropore surface area is well correlated with the dilution effect caused by incorporation of 30 wt% attapulgite, taking into account that the latter has no microporosity. This result denotes that both the integrity and accessibility of the ZSM-5 micropores are maintained after the agglomeration process.

The acid and base properties of the catalysts were evaluated by NH_3 and CO_2 temperature-programmed desorption (TPD), respectively (see Table 1). Incorporation of ZrO_2 into zeolite n-ZSM-5 increased the overall acidity owing to the generation of a new type of acidic sites, which also had an enhancement effect on the concentration of basic sites. These findings can be directly assigned to the amphoteric properties of ZrO_2. In contrast, the agglomeration with attapulgite barely altered the overall catalyst acidity, although it increased the concentration of basic sites, which has been previously related to the interaction of Mg^{2+} species, migrating from the attapulgite, with both the zeolitic and ZrO_2 components.[36] Accordingly, the technical ZrO_2/n-ZSM-5-ATP catalyst exhibits singular acid–base properties, showing a combination of Brønsted and Lewis acidity as well as basic sites.

Figure 1 illustrates the SEM and TEM images of the different materials employed for the preparation of the technical catalyst. The binder-free n-ZSM-5 and ZrO_2/n-ZSM-5 samples are formed of nanocrystallites of approximately 40–60 nm, aggregated into 20–50 μm particles,[35] whereas attapulgite shows its characteristic needle-like morphology[37,38] as well as some impurities associated with quartz (highlighted in the image).

Table 1. Physicochemical properties of the zeolite ZSM-5-based samples.

Catalyst	Si/Al[a]	ZrO_2 [wt%]	S_{BET}[b] [$m^2 g^{-1}$]	$S_{MES+EXT}$[c] [$m^2 g^{-1}$]	S_{MIC}[d] [$m^2 g^{-1}$]	V_T[e] [$cm^3 g^{-1}$]	V_{MIC}[f] [$cm^3 g^{-1}$]	Acidity[g] [mmol g^{-1}]	Basicity[h] [μmol g^{-1}]
n-ZSM-5	42	–	445	133	312	0.512	0.186	0.28	3.26
ZrO_2/n-ZSM-5	42	9.2	395	105	290	0.620	0.173	0.39	11.01
ZrO_2/n-ZSM-5-ATP	42	10.5	325	102	223	0.445	0.133	0.38	18.39

[a] Si/Al ratio of the zeolite component, measured by ICP-OES. [b] Brunauer–Emmett–Teller (BET) surface area. [c] Mesopore and external surface area. [d] Micropore surface area. [e] Total pore volume at $P/P_0 \approx 0.98$. [f] Micropore volume. [g] Measured by TPD-NH_3. [h] Measured by TPD-CO_2.

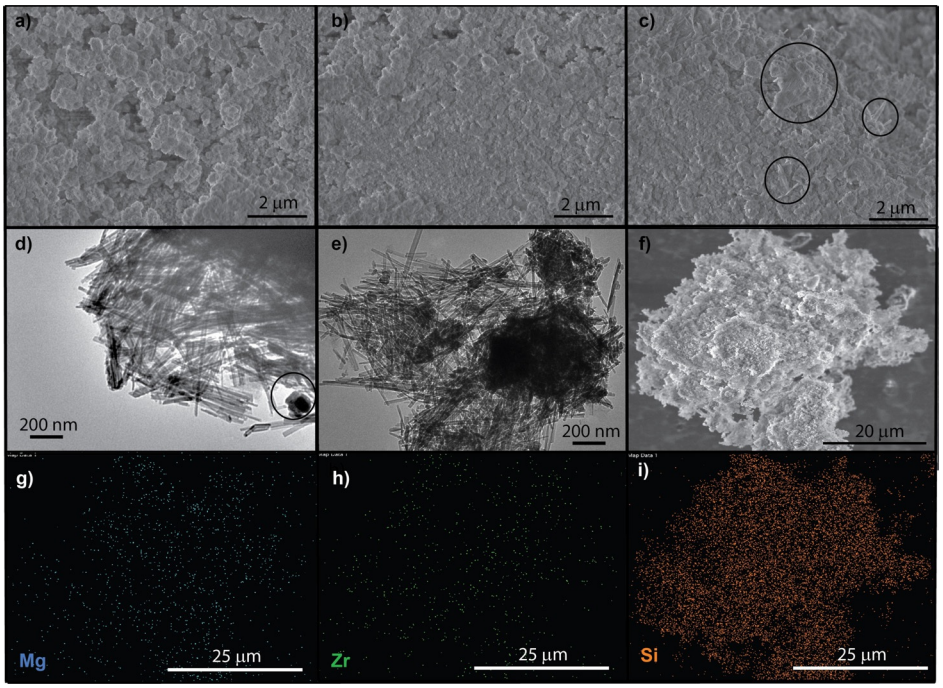

Figure 1. SEM (a–c) and TEM (d,e) images of (a) n-ZSM-5, (b) ZrO_2/n-ZSM-5, (d) ATP, and (c,e) ZrO_2/n-ZSM-5-ATP. (f–i) SEM and derived elemental EDX dot maps for ZrO_2/n-ZSM-5-ATP.

SEM-energy-dispersive X-ray (EDX) analysis of the ZrO_2/n-ZSM-5-ATP catalyst Figure 1e–i shows that Zr was evenly distributed over the sample, as evident from EDX dot-mapping, with a Si/Zr molar ratio of approximately 43 (Figure S1 in the Supporting Information). The Zr content of the ternary sample was slightly lower than that of the ZrO_2/n-ZSM-5 catalyst ($\approx$14, blue series Figure S1 in the Supporting Information) owing to both the dilution of the material with attapulgite and to the newly incorporated Si naturally present in the clay. Likewise, Mg was also found to be very homogeneously distributed along the catalyst surface (Si/Mg$\approx$21), indicative of an even zeolite/clay distribution.

Figure S2 (in the Supporting Information) shows the XRD pattern of the ZrO_2/n-ZSM-5-ATP catalyst, compared with the parent materials, the pure zeolite n-ZSM-5, and impregnated ZrO_2/n-ZSM-5. The ternary catalyst, just as the parent materials, shows the orthorhombic phase of the MFI framework (*Pnma*, PDF 00-044-0003),[39,40] whereas ZrO_2 is X-ray invisible as a result of the lack of crystallinity of the ZrO_2 nanoparticles and/or their small size.[35] The attapulgite phase is evident from the XRD of the ZrO_2/n-ZSM-5-ATP catalyst by the presence of a small amount of quartz phase, a common impurity of this clay also detected by TEM (Figure 1d), at $2\theta = 31.1^\circ$ (Figure S2c in the Supporting Information).

Aluminum speciation was examined by solid-state ^{27}Al magic-angle spinning (MAS; Figure 2a) and ^{27}Al multiple-quantum (MQ) MAS NMR (Figure 2b) analyses. Zeolite n-ZSM-5 (black series) contains almost exclusively tetrahedrally coordinated Al species, located at 54 ppm, and very little presence of octahedrally coordinated Al (signal at 0 ppm).[41–43] The same is seen after ZrO_2 addition (green series), with the NMR spectrum of ZrO_2/n-ZSM-5 practically identical to that of the pure zeolite.

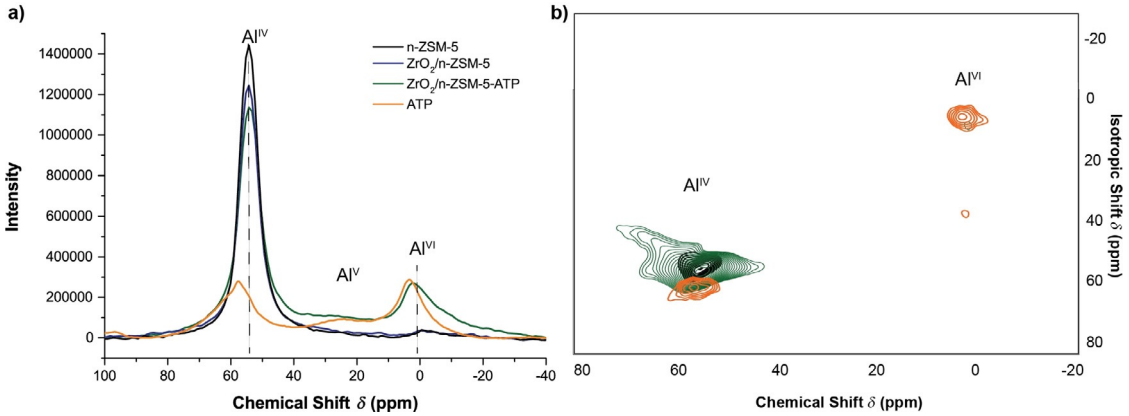

Figure 2. (a) ^{27}Al MAS solid-state NMR spectra of n-ZSM-5 (black), ZrO_2/n-ZSM-5 (blue), ZrO_2/n-ZSM-5-ATP (green), and ATP (orange). (b) Overlapping of ^{27}Al MQ MAS solid-state NMR spectra. $\pi/12$ ^{27}Al pulse excitation source (0.87 µs), MAS 18 kHz, T_{set} 298 K.

The lower intensity of the resonance at 54 ppm is caused by the incorporation of 9.2 wt% ZrO_2. Attapulgite (orange series), which contains approximately 5 wt% Al, presents different Al species: tetrahedral at approximately 62[44] and 58 ppm, penta-coordinated at 25 ppm, and octahedral at 3 ppm.[45] The mixing of ZrO_2/n-ZSM-5 with attapulgite and the further extrusion leads to changes in the Al environment.[46] The framework Al^{IV} species, at 54 ppm, suffer some distortion as evident from the broadening and increase in anisotropy of the resonance for the ternary ZrO_2/n-ZSM-5-ATP catalyst. At the same time, an enhancement in the extra-framework Al occurs, as evident from the hump at 35–25 ppm assigned to penta-coordinated Al^{V} species, and the increase in octahedral Al^{VI} species, which appear at higher chemical shift (≈2 ppm; Figure 2a).

The 4-fluorostyrene oligomerization reaction was performed to study the effect of attapulgite on Brønsted acidity and catalyst accessibility.[47–50] In the reaction catalyzed by ZrO_2/n-ZSM-5-ATP (Figure 3a,b), styrene oligomers were formed, but to a lower extent than over the n-ZSM-5 (Figure 3c) and ZrO_2/n-ZSM-5 (Figure 3d) catalysts. The intensity evolution of the cyclic oligomers (**7**), favored in zones with high densities of Brønsted acid sites, was particularly low for the ZrO_2/n-ZSM-5-ATP catalyst. On the contrary, the formation of linear dimer (**5**) was more pronounced, especially in the first 5 min of the reaction; afterwards, the relative amount of trimer oligomers (**6a** and **6b**) increased.

The evolution of band intensities for the three catalysts and the related profiles obtained (Figure 3a) indicate a progressive loss in Brønsted acidity suffered by the zeolite n-ZSM-5 upon ZrO_2 addition and especially after attapulgite inclusion. This can be visually confirmed by the images shown in Figure S3 (in the Supporting Information). The optical images vary in color from light to dark pink and finally to violet for n-ZSM-5 (Figure S3a), ZrO_2/n-ZSM-5 (Figure S3b), and ZrO_2/n-ZSM-5-ATP (Figure S3c), respectively. This indicates a higher presence of cyclic oligomers (**7**) with absorption bands evolving at 515 nm for the n-ZSM-5 catalyst, and a higher presence of linear dimers (**5**) with absorption bands evolving at 555 nm for ZrO_2/

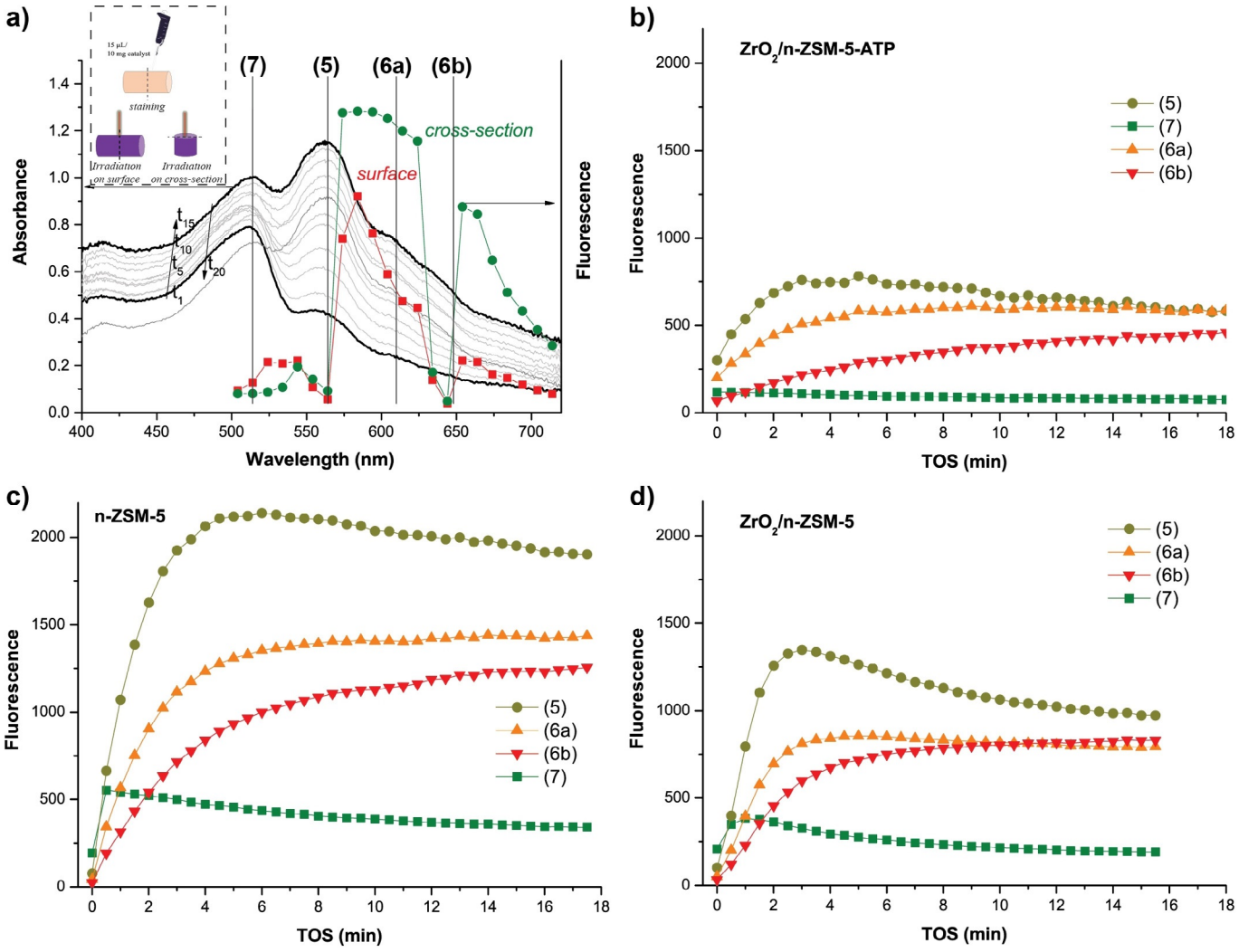

Figure 3. (a) In situ absorption UV/Vis (continuous line) and ex situ fluorescence spectra (scattered line; red for recorded on surface, green for cross-section) of the 4-fluorostyrene oligomerization reaction products recorded at 100 °C on ZrO_2/n-ZSM-5-ATP. Inset: scheme of the impregnation and recording process. Evolution of emission bands during reaction for (b) ZrO_2/n-ZSM-5-ATP, (c) n-ZSM-5, and (d) ZrO_2/n-ZSM-5, for the sake of comparison. Excitation lasers are fixed at $\lambda = 488$, 561, and 642 nm.

n-ZSM-5-ATP. Complementary confocal fluorescence microscopy pictures demonstrate that the fluorescence ranges from green to more orange-like (Figure S3 e–g in the Supporting Information). Note that pure attapulgite, which cannot catalyze this styrene oligomerization reaction given its lack of Brønsted acidity, does not change in color (Figure S3 d in the Supporting Information) and, hence, does not undergo any fluorescence in the presence of the styrene monomer, as indicated by the black confocal fluorescence image (Figure S3 h in the Supporting Information). The partial loss of Brønsted acidity after agglomeration with attapulgite has been reported previously, although this effect is compensated by an increase in the amount of Lewis acid sites.[36]

The ZrO_2/n-ZSM-5-ATP extrudate shows good accessibility, as demonstrated by confocal fluorescence microscopy. The ex situ emission spectrum taken on the cross-section of the catalyst after reaction (green scattered series, Figure 3 a, right axis) shows more intense fluorescence that the one taken on the surface on which the catalyst staining was performed (red series). This observation confirms the good diffusivity/accessibility of the nanocrystalline ZrO_2/n-ZSM-5-ATP extrudate for styrene derivatives.

Biomass catalytic pyrolysis

Laboratory-scale tests

The activity of the ZrO_2/n-ZSM-5-ATP catalyst was tested in wheat straw catalytic pyrolysis by using an ex situ laboratory-scale reactor with different reaction temperatures in the thermal (550 °C) and catalytic (400 °C) zones, operating in batch mode by discharging at once 4 g of biomass into the reactor. To avoid interferences from the inorganic components present in the raw biomass, which could act as indigenous catalysts favoring the formation of char in detriment to the bio-oil yield, the wheat straw was subjected to an acid-washing pre-treatment affording the removal of 98 wt% of the alkaline and alkaline earth metals (AAEM), denoted as WS-ac. A detailed description of the properties of this biomass can be found elsewhere.[10,26]

The performance of the ZrO_2/n-ZSM-5-ATP material in the catalytic pyrolysis of de-ashed wheat straw was tested by using six C/B ratios (0.1, 0.2, 0.3, 0.4, 0.5, and 0.7 $g\,g^{-1}$) to obtain insights about the progression of the pyrolysis vapors upgrading as a function of the catalyst loading. In the reactor configuration herein employed, the residual solid fraction (char), which originates entirely from the initial biomass decomposition, is retained in the upper reactor zone, avoiding direct contact with the catalyst bed. The char yield was approximately 19 wt% for all experiments, independent of the C/B ratio.

Figure 4 a illustrates the product distribution, in terms of mass yield, corresponding to the different fractions (char excluded) as a function of the C/B ratio. The products herein displayed include the non-condensable gases, the liquid phases, and the coke deposited over the catalyst. The liquid fraction is separated in water and bio-oil on a dry basis (bio-oil*). The results obtained in a pure thermal test, performed with no catalyst, are also included in this graph as a reference. Likewise, the oxygen content of the bio-oil fraction is shown in Figure 4 b.

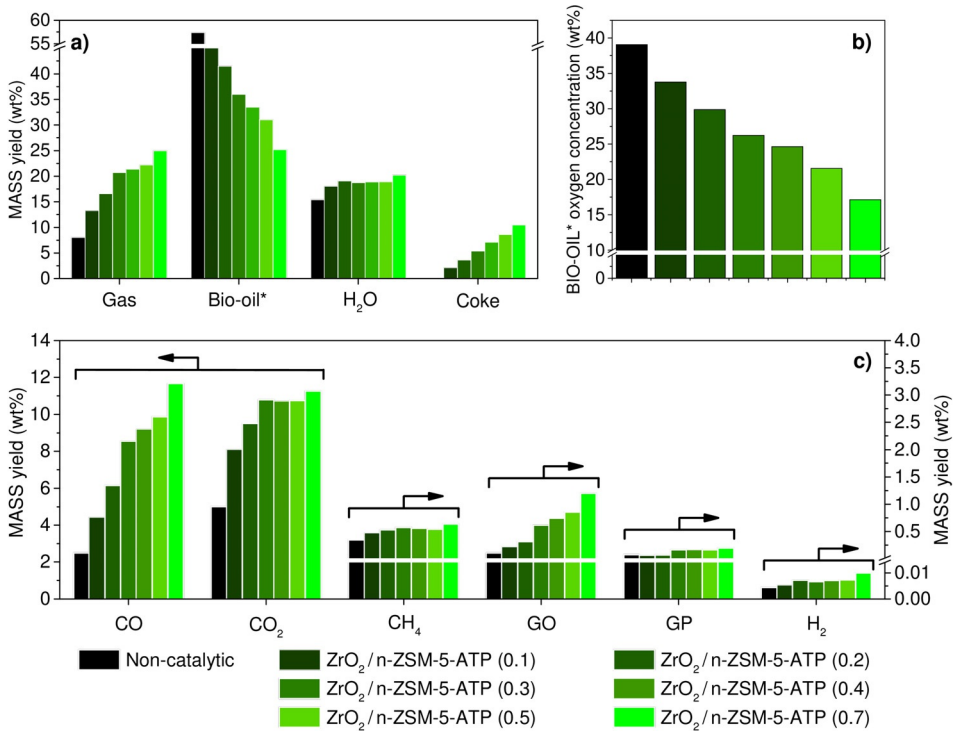

Figure 4. (a) Product yield distribution, (b) bio-oil oxygen concentration, and (c) gaseous component yield, obtained in the WS-ac pyrolysis over ZrO_2/n-ZSM-5-ATP by using different C/B ratios. GO: gaseous olefins (C_2–C_4); GP: gaseous paraffins (C_2–C_4).

In line with previous studies,[10,35] the presence of the catalyst caused strong changes in the yield of the different fractions compared with the pure thermal test. A strong decrease of the bio-oil yield and an enhancement in the production of non-condensable gases and water was observed, in addition to the formation of coke over the catalyst. These variations were accompanied by a significant reduction in the oxygen content of bio-oil, from approximately 39 wt% (thermal test) to 17 wt% (catalytic test with C/B = 0.7 g g^{-1}), showing the effectiveness of the catalyst in promoting deoxygenation reactions. Using progressively higher C/B ratios led to increased bio-oil deoxygenation but also to higher production of gases and coke, at the expense of the bio-oil yield. The water yield did not change significantly over the whole range of C/B values, denoting that the catalyst here employed does not specifically favor dehydration reactions.

The main components present in the gaseous fraction include CO, CO_2, CH_4, gaseous olefins (GO), and gaseous paraffins (GP), and their yields are shown in Figure 4c as a function of the C/B ratio. For all gases, the yield increased with the C/B ratio, but with two different patterns. In the case of CO and gaseous olefins, the yield variation was more or less proportional to the C/B ratio. However, for CO_2, methane, gaseous paraffins, and hydrogen, the yield increase was pronounced for C/B up to 0.2, suggesting that the species and functional groups that generate these products are mainly consumed in the initial steps of the biomass catalytic pyrolysis process. As shown in Table 2, methane is the predominant component within gaseous paraffins, whereas propylene is the major one within gaseous olefins over the whole range of C/B ratios investigated.

Table 2. Mass yield of gaseous hydrocarbons obtained in the WS-ac pyrolysis over ZrO_2/n-ZSM-5-ATP by using different C/B ratios.

Catalyst	Light paraffins [wt% × 10^{-2}]				Light olefins [wt% × 10^{-2}]		
	CH_4	C_2H_6	C_3H_8	C_4H_{10}	C_2H_4	C_3H_6	C_4H_8
non-catalytic	34.3	5.6	2.0	0.4	5.5	4.5	0.4
ZrO_2/n-ZSM-5-ATP (0.1)	47.2	3.2	3.0	0.7	11.1	10.6	0.8
ZrO_2/n-ZSM-5-ATP (0.2)	53.3	3.1	3.4	3.9	12.6	18.5	1.6
ZrO_2/n-ZSM-5-ATP (0.3)	57.2	12.0	4.3	4.9	22.7	38.9	6.6
ZrO_2/n-ZSM-5-ATP (0.4)	55.2	11.9	4.3	5.4	26.7	47.0	7.8
ZrO_2/n-ZSM-5-ATP (0.5)	54.0	12.0	4.4	5.9	30.6	54.8	8.1
ZrO_2/n-ZSM-5-ATP (0.7)	63.8	14.1	5.6	7.8	45.9	74.1	11.1

As shown in Figure 4a, the yield of the coke deposited over the catalyst increased almost linearly with the C/B ratio. Note that these values refer to the initial biomass weight, reaching approximately 10 wt% at the highest C/B ratio. Therefore, if char and coke are grouped together, it means that for this C/B ratio approximately 29 wt% of the biomass was transformed into carbonaceous residues, denoting the relevance of minimizing the production of these fractions as well as finding applications for them. In this context, both char and coke could be combusted to provide a great part of the energy consumed in the overall catalytic pyrolysis process. Thus, Table 3 discloses

Table 3. Char and coke composition, and corresponding HHV values, obtained for the WS-ac pyrolysis over ZrO_2/n-ZSM-5-ATP by using different C/B ratios.

Compound	C/B ratio	Coke over catalyst[a] [wt%]	Ultimate analysis [wt%]				HHV [MJ kg^{-1}]
			C	H	N	O	
char[b]	–	–	72.1	2.7	0.8	5.3	27.4
coke	0.1	13.1	58.7	5.7	1.0	34.6	23.6
coke	0.2	12.6	56.2	5.0	1.3	37.5	21.6
coke	0.3	12.5	49.9	5.4	0.6	44.7	19.2
coke	0.4	12.4	52.3	4.3	0.6	43.4	18.8
coke	0.5	12.1	47.1	4.9	0.5	48.1	17.2
coke	0.6	10.5	55.9	5.7	0.2	38.4	22.2

[a] Based on ZrO_2/n-ZSM-5-ATP. [b] Char proximate analysis: vol. = 12.8 wt%; ash = 19.0 wt%; fixed carbon = 68.2 wt%.

the composition of char and coke, their high heating values (HHVs), and the amount of coke referenced to catalyst weight. Regarding the char, the data indicate that this fraction accumulated most of the ash still contained in the raw biomass, but it had little oxygen and therefore possessed a relatively high HHV. In the case of the coke deposits, it is interesting to note that the amount of coke expressed per gram of catalyst decreased with the C/B ratio, but in a small range, from 13.1 (C/B = 0.1) to 10.5 wt% (C/B = 0.7), which suggests that its formation is limited by the porosity of the catalyst. One other interesting fact is that the coke composition was very different to that of the char, showing lower C and H amounts, similar N content, and higher amounts of O, which in turn led to lower HHV. These results point out that the zeolite-based catalyst tends to accumulate highly oxygenated compounds. The oxygen contents of the coke deposits exhibited a maximum at a C/B ratio of 0.5, whereas the N proportion decreased continuously, which evidences some changes in the nature of the species retained over the catalyst.

Bio-oil deoxygenation takes place through a complex scheme of reactions that lead to the generation of water, CO, and CO_2 as the final products according to three main deoxygenation routes, respectively: dehydration, decarbonylation, and decarboxylation. With the aim of preserving as much as possible of the chemical energy of the bio-oil and increasing its H/C ratio, decarboxylation should be the preferred route. Figure 5a shows the changes in the overall deoxygenation selectivity towards the three routes with increasing C/B ratio, defined as the mass of oxygen in the form of CO, CO_2, or H_2O, respectively, referenced to the total amount of oxygen present in these three compounds. The most pronounced one is dehydration, followed by decarboxylation, and finally decarbonylation. However, it must be taken into account that a great part of the formation of water, CO_2, and CO occurs during the thermal step, which causes little deoxygenation of the bio-oil phase, its effect being in reality reflected in the composition of the char fraction, which possesses a low oxygen content as indicated above. Accordingly, the deoxygenation selectivity of the catalytic step has been defined similarly to the overall selectivity but taking into account the incremental production of

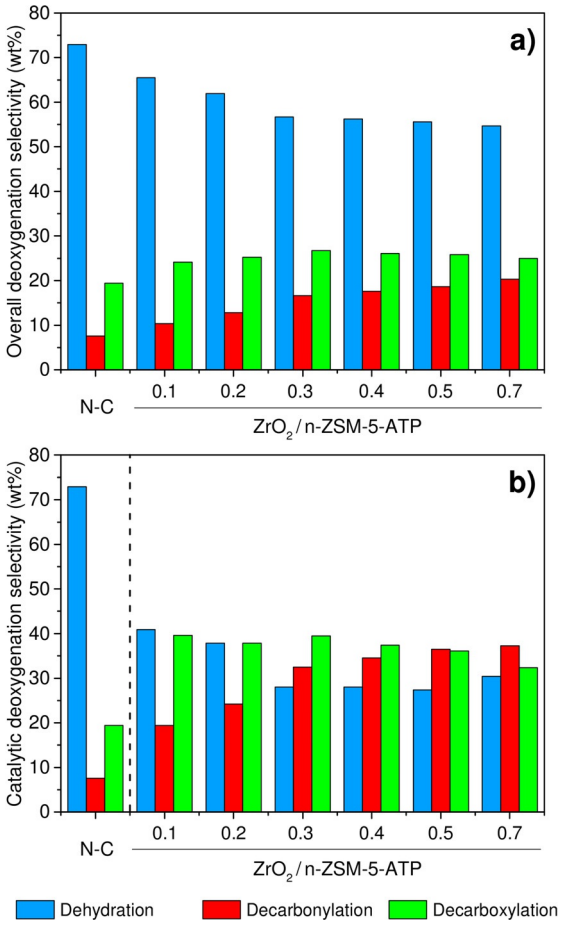

Figure 5. (a) Overall deoxygenation selectivity and (b) catalytic deoxygenation, obtained in the WS-ac pyrolysis over ZrO_2/n-ZSM-5-ATP by using different C/B ratios. N-C: non-catalytic.

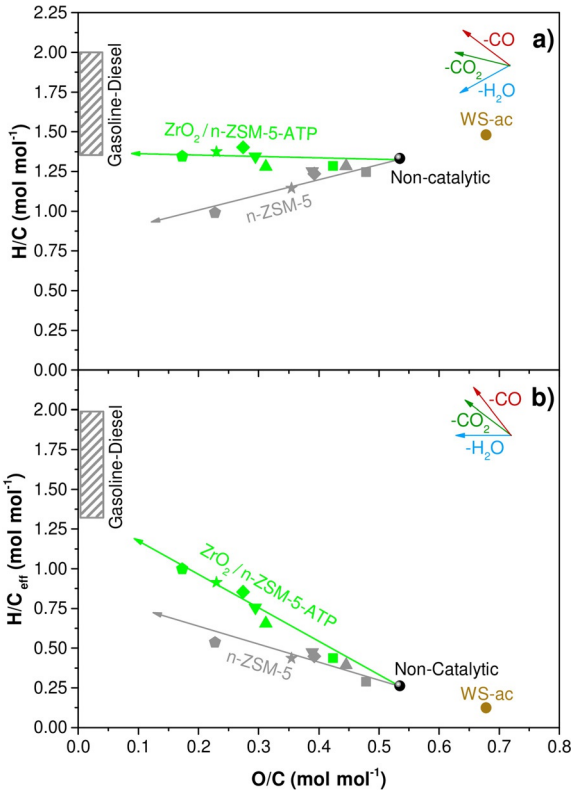

Figure 6. Van Krevelen graphs obtained for the WS-ac pyrolysis over ZrO_2/n-ZSM-5-ATP in comparison with the parent zeolite n-ZSM-5, by varying the C/B ratio.

CO, CO_2, or H_2O, which take place when the vapors generated in the thermal zone are passed through the catalyst bed. Thereby, the results obtained in the pure thermal test have been taken as the reference. The deoxygenation selectivity of the catalytic step is more representative of the bio-oil deoxygenation pathways than the overall one. As shown in Figure 5, and in contrast with non-catalytic pyrolysis, in which dehydration is by far the predominant deoxygenation route, the use of ZrO_2/n-ZSM-5-ATP leads to a quite balanced scheme. Thus, for C/B = 0.1, dehydration and decarboxylation contribute to an almost similar extent, followed by decarbonylation. However, at higher C/B ratios the decarbonylation selectivity increases progressively, becoming the major route for C/B = 0.7. These results denote that the bio-oil deoxygenation promoted by the catalyst is a balanced combination of the three routes, the relative contributions of which vary with the C/B ratio.

The variation of the elemental composition of the bio-oil in the tests performed by using different catalyst loadings is shown in Figure 6a,b in the form of van Krevelen graphs, representing the overall and effective H/C ratios versus the O/C ratio, respectively. The latter has been defined in earlier works[51,52] as $H_{eff}/C = (H-2O-3N-2S)/C$ to account only for the hydrogen that could be finally available if all the oxygen present in the bio-oil is removed in the form of water. The results obtained with the parent zeolite n-ZSM-5 are also included as a reference. According to Figure 6a, for ZrO_2/n-ZSM-5-ATP, passing from the raw biomass first to the thermal bio-oil and then to that produced in the catalytic pyrolysis tests involves a significant reduction in the O/C ratio, whereas the overall H/C ratio just slightly increases. However, the emerging picture is more positive upon assessing the results obtained in the form of H_{eff}/C (Figure 6b) because they show a clearly increasing trend, which approaches progressively the composition region typical of fossil-derived fuels. Interestingly, the pathways followed in the van Krevelen graphs for the parent n-ZSM-5 catalyst are less favorable compared with the catalyst investigated here, with a reduction in the values of the overall H/C ratio and a lower increase in the H_{eff}/C. These results denote the positive effects caused by the modification of zeolite ZSM-5 by incorporation of ZrO_2 and agglomeration with attapulgite in terms of bio-oil composition upgrading aimed at the production of advanced biofuels. More detailed information about the elemental compositions of the bio-oils* can be found in Table S1 (in the Supporting Information).

Another essential parameter to be taken into consideration in biomass catalytic pyrolysis is the energy yield, which reveals how the chemical energy initially contained in the raw biomass is shared among the different pyrolysis products. Figure 7 illustrates the energy yield corresponding to the different fractions obtained in the catalytic pyrolysis process and its variation

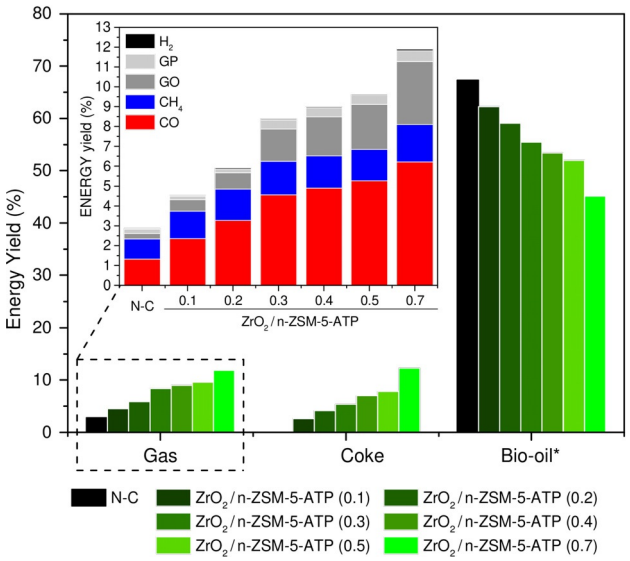

Figure 7. Energy yield distribution obtained in the WS-ac pyrolysis over ZrO_2/n-ZSM-5-ATP as a function of the C/B ratio (0.1–0.7 g g^{-1}).

with the increase of the C/B ratio. The bio-oil energy yield decreases continuously with the C/B ratio, whereas the opposite occurs with the chemical energy contained in the gases and coke. Within the gaseous fractions, more than half of the chemical energy corresponds to CO, followed by light olefins, methane, and light paraffins, whereas the contribution of hydrogen is almost negligible owing to its low concentration.

The above results demonstrate that the variation of the C/B ratio is effective for invoking the bio-oil upgrading through deoxygenation reactions, but this parameter also includes significant losses in terms of both mass and energy yields, mainly owing to the occurrence of a variety of non-desired secondary transformations. The relationship between oxygen content and yield of the bio-oil fraction upon varying the C/B ratio is illustrated in Figure 8, comparing again the results obtained with the catalyst investigated here and those corresponding to the parent zeolite n-ZSM-5. This figure highlights the relevance of fine-tuning the zeolite properties to improve its performance in the biomass catalytic pyrolysis. For the parent n-ZSM-5, bio-oil deoxygenation implies a sharp reduction in both mass and energy yield. In contrast, these negative effects are less pronounced for ZrO_2/n-ZSM-5-ATP. Thus, for a bio-oil oxygen content of approximately 22 wt%, the bio-oil energy yield corresponding to the parent zeolite is just 34%, whereas it increases up to 52% over the modified ZSM-5 catalyst. Moreover, with the latter catalyst it is possible to reach deoxygenation levels of the bio-oil superior to those of the parent n-ZSM-5, reducing the bio-oil oxygen content to values as low as 17 wt% and still retaining 45% of the chemical energy initially present in the raw biomass. These results denote that modification of the zeolite ZSM-5 with ZrO_2 and attapulgite leads to a significantly more efficient pathway during the bio-oil upgrading process.

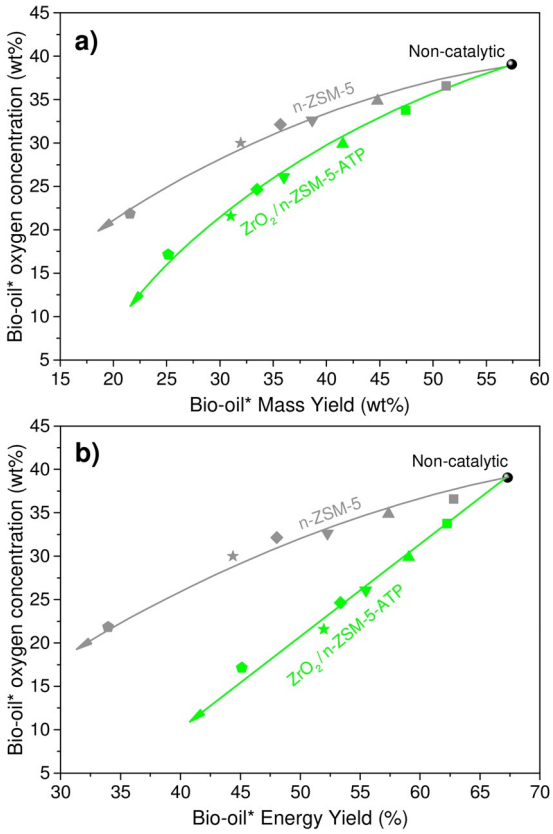

Figure 8. Bio-oil* oxygen concentration versus (a) mass and (b) energy yields obtained in the WS-ac pyrolysis over ZrO_2/n-ZSM-5-ATP in comparison with those corresponding to the parent zeolite n-ZSM-5, by varying the C/B ratio.

Bench-scale tests

To validate the promising performance of ZrO_2/n-ZSM-5-ATP on a larger scale, ex situ biomass catalytic pyrolysis tests were performed in a bench-scale unit, working with continuous biomass feeding at different C/B ratios (0.20, 0.25, 0.43, and 0.50 g g^{-1}). In these tests, the catalyst loading was varied in the range 20–50 g, that is, an order of magnitude higher than the catalyst amount used for the laboratory-scale tests reported above.

Figure 9 compares the mass yield of the main products obtained by using ZrO_2/n-ZSM-5-ATP in the laboratory and bench plant experiments for two C/B ratios. A deeper conversion of the bio-oil fraction occurred for the tests performed in the bench plant, as denoted by the lower bio-oil yield as well as by its reduced oxygen content. For both scales, increasing the C/B ratio provoked a progressive reduction of the bio-oil yield, which was accompanied by a decrease of its oxygen content. For the bench reaction system, a higher production of the different gaseous components was observed: methane, olefins, paraffins, and especially CO and CO_2. However, the water yield was very similar in both series of experiments, remaining almost constant with respect to the variation of the C/B ratio, which confirms that the employed catalyst promotes to a higher extent decarboxylation and decarbonylation reactions rather than dehydration reactions.

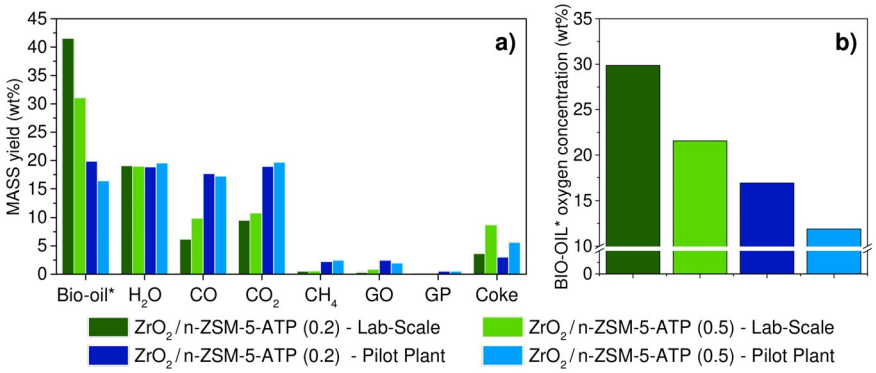

Figure 9. (a) Product yield distribution and (b) bio-oil oxygen concentration, obtained for biomass pyrolysis at both laboratory and bench plant scales over ZrO_2/n-ZSM-5-ATP by using different C/B ratios (0.2 and 0.5).

The differences between the results obtained in the two experimental sets up can be assigned mainly to the longer residence time of the bio-oil vapors, in addition to the higher temperature of the catalytic bed, for the bench scale, which provokes a more pronounced conversion and deoxygenation of the bio-oil in comparison with the laboratory-scale system. In this way, it must be noted that the biomass pyrolysis proceeds on the laboratory scale in two separated zones (thermal and catalytic) located within the same reactor, whereas in the case of the bench plant the thermal pyrolysis and the catalytic upgrading steps take place in two different reactors connected in series. This fact leads to significant differences in the residence times of the bio-oil vapors in the respective thermal zones ($\approx$1 s in the laboratory setup vs. 7 s in the bench-scale plant), whereas the residence times in both catalytic beds are very similar (in the range 0.5–1 s).

Regarding the coke deposited over the catalyst, its yield was more pronounced at higher C/B ratios, with a higher quantity forming in the case of the laboratory-scale tests. This negative effect was counterbalanced by the decreasing amount of oxygen in the liquid organics with increasing catalyst loading in the upgrading reactor. Thus, for the bench-plant experiments, at the highest C/B ratio investigated (0.5 $g\,g^{-1}$), a very good quality bio-oil with only 10 wt% oxygen content was produced at a mass yield of approximately 16 wt%, which corresponds to approximately one third of the initial chemical energy in the biomass feedstock.

For comparing the relationship between the yield and oxygen content of the bio-oil obtained at lab and bench scales, it is important to take into account that the starting point, that is, the yield and composition of the thermal bio-oil, is different in both series of tests. Accordingly, the deoxygenating degree of the bio-oil attained in the catalytic upgrading step has been referenced to the oxygen content of the thermal bio-oil. In the same way, the energy yield of the bio-oil has been computed, taking as a reference those corresponding to the bio-oils produced in absence of catalyst for both series of experiments. Accordingly, Figure 10 compares the relationship between the bio-oil deoxygenation degree and its energy yield, referenced to those of the thermal bio-oils, providing thus information on the catalytic effects of the ZrO_2/n-ZSM-5-ATP system for upgrading the organics produced in the thermal zones of the corresponding reaction systems. It can be observed that both series of points exhibit a similar trend in spite of the differences in the conditions and sets up between them. This is a remarkable result because it demonstrates that the ZrO_2/n-ZSM-5-ATP system exhibits similar catalytic properties for different raw biomasses, reaction conditions, and operation modes, providing deoxygenation degrees up to 60% with energy yields of approximately 70% with respect to those of the thermal bio-oils. Moreover, it can be concluded that this excellent performance is maintained upon scaling up the process from batch laboratory system to a continuous bench plant.

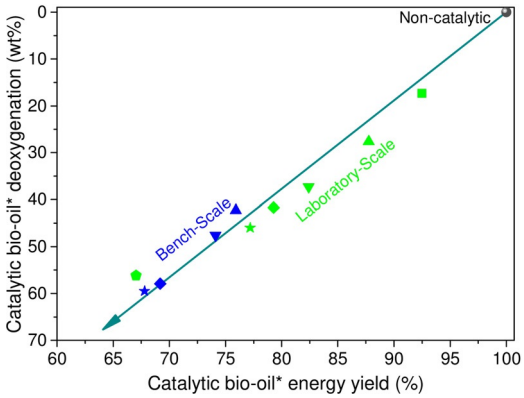

Figure 10. Bio-oil* deoxygenation degree versus bio-oil energy yield of the catalytic step (referenced to those of the thermal bio-oil), obtained for biomass pyrolysis at laboratory and bench scales over ZrO_2/n-ZSM-5-ATP by using different C/B ratios.

The actual liquid biofuel obtained from the bench plant tests was collected and analyzed to determine its suitability for use in fuel applications. It should be noted that the total liquid product produced from thermal biomass pyrolysis followed by upgrading of the vapors in the consecutive catalytic reactor segregated into two phases: an aqueous light phase, containing mainly water and a low amount of polar organic compounds, and an organic-rich heavy phase, with low moisture and high organics content. This organic phase was separated from the aqueous phase for the tests at C/B ratios 0.25 and

Table 4. Characterization of the bio-oil organic phase obtained from oak pyrolysis at the bench scale over ZrO_2/n-ZSM-5-ATP.

C/B	Percentage of total liquid product [%]	H_2O [wt%]	Elemental composition [wt% d.b.] C	H	O	TAN [$mg_{KOH}\,g^{-1}$]	HHV [$MJ\,kg^{-1}$ d.b.]	Energy yield [%]
0.25	45.8	3.6	80.6	7.3	12.0	8.5	35.8	33.0
0.50	42.8	2.7	83.5	7.6	8.8	2.6	37.6	30.2

d.b.: dry basis.

0.50 and was characterized to determine its water content, elemental composition, total acid number (TAN), and heating value. These results, together with the percentage of the organic phase in the total liquid, are summarized in Table 4. This organic phase has favorable properties for fuel use because it has little water, and the oxygen content is very low compared with typical pyrolysis bio-oil without the use of hydrogen in the process and merely resulting from the effective deoxygenation induced by ZrO_2/n-ZSM-5-ATP. This is also reflected in the high heating value, which is close to that of fossil-based fuels. Another important property for fuel applications is the TAN, which corresponds to the acidity, and thus corrosiveness, of the fuel. In the case of both organic liquids, the TAN is very low owing to the effective removal of oxygen from the acidic molecules in the bio-oil vapors.

The organic phase of the bio-oil sample obtained from the bench-scale pyrolysis tests at a C/B ratio of 0.25 was also analyzed by GC–MS to determine the composition of the produced liquid. The bio-oil compounds were identified and grouped in families according to their functional groups. Figure 11 shows the semi-quantitative GC–MS results (expressed as percentage of relative area) in terms of the main chemicals groups. The organic bio-oil consists mainly of aromatic, phenolic, and aliphatic compounds, as well as polyaromatic hydrocarbons, consistent with the high deoxygenation activity of ZrO_2/n-ZSM-5-ATP, which resulted in the production of bio-oil with low oxygen content and high heating value. Moreover, the amount of oxygenates, such as aldehydes, ketones, and acids, is very low, also indicative of the efficiency of this catalyst and in line with the reduced TAN of the biofuel.

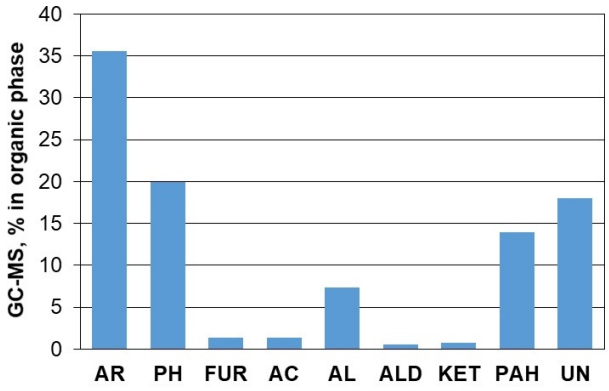

Figure 11. Semi-quantitative analysis of the organic phase of bio-oil obtained in the fast pyrolysis of lignocellulosic biomass at the bench scale over ZrO_2/n-ZSM-5-ATP at a C/B ratio of 0.25 with GC–MS. AR: aromatic compounds; PH: phenolic compounds; FUR: furanic compounds; AC: acids; AL: aliphatic compounds; ALD: aldehydes; KET: ketones; PAH: polyaromatic hydrocarbons; UN: unidentified compounds.

Conclusions

The ZrO_2/n-ZSM-5-ATP material is an efficient catalyst for the upgrading of the bio-oil vapors produced by biomass pyrolysis by using an ex situ configuration. In addition to high accessibility for bulky molecules, provided by the nanocrystalline nature of the ZSM-5 sample, this material exhibits the right balance of acidic and basic sites, which is essential for catalyzing the variety of reactions taking place during biomass pyrolysis and bio-oil upgrading. As a consequence, the ZrO_2/n-ZSM-5-ATP catalyst led in the laboratory scale tests to a quite more selective deoxygenation pathway upon variation of the catalyst-to-biomass ratio, as denoted by the improved relationship between the bio-oil yield and its oxygen content in comparison with that of the parent n-ZSM-5 sample. Likewise, the pathways followed in the van Krevelen graphs for using the parent n-ZSM-5 catalyst are less favorable compared with the catalyst material here investigated, with a reduction in the values of the overall H/C ratio and a smaller increase in the H_{eff}/C ratio, which confirms the remarkable positive effects derived from the zeolite modification by ZrO_2 impregnation and agglomeration with attapulgite. In the bench-scale tests, performed by using the ZrO_2/n-ZSM-5-ATP catalyst, a lower bio-oil yield was obtained although it also showed lower oxygen content in comparison with the laboratory-scale results. These differences can be assigned mainly to the longer residence time of the bio-oil in the bench-scale test, which led to a more pronounced conversion and deoxygenation of the bio-oil.

Interestingly, the ZrO_2/n-ZSM-5-ATP system exhibits similar catalytic properties for upgrading the thermal bio-oil vapors even for different raw biomasses, reaction conditions, scales, and operation modes, providing deoxygenation degrees up to 60% with energy yields of approximately 70% with respect to those of the thermal bio-oils. Moreover, this finding confirms the feasibility of upscaling the biomass catalytic pyrolysis process from laboratory to bench scale.

Experimental Section

Detailed information about the preparation of the catalysts and characterization techniques used, as well as information on the procedure and setups employed for the biomass catalytic pyrolysis tests, is provided in the Supporting Information.

Acknowledgements

The authors gratefully acknowledge financial support from the European Union Seventh Framework Program (FP7/2007–2013) under grant agreement no. 604307 (CASCATBEL project), and from the Spanish Ministry of Economy and Competitiveness through CATPLASBIO project (Ref: CTQ2014-602209). R. J. Wijten (Utrecht University, UU) is acknowledged for performing the SEM-EDX measurements. Dr. K. Houben (UU) and Prof. M. Baldus (UU) are thanked for carrying out the ^{27}Al (MQ) MAS NMR measurements.

Conflict of interest

The authors declare no conflict of interest.

Keywords: biomass · bio-oil · catalytic pyrolysis · pyrolysis · ZSM-5

[1] A. V. Bridgwater, *Biomass Bioenergy* **2012**, *38*, 68 – 94.
[2] J. Fermoso, P. Pizarro, J. M. Coronado, D. P. Serrano, *Adv. Rev.* **2017**, *6*, 1 – 18.
[3] J. Fermoso, P. Pizarro, J. M. Coronado, D. P. Serrano, *Transportation Biofuels via the Pyrolysis Pathway: Status and Prospects in Encyclopedia of Sustainability Science and Technology* (Ed.: R. A. Meyers), Springer, New York, **2017**, pp. 1 – 33.
[4] C. Liu, H. Wang, A. M. Karim, J. Sun, Y. Wang, *Chem. Soc. Rev.* **2014**, *43*, 7594 – 7623.
[5] A. V. Bridgwater, *Catal. Today* **1996**, *29*, 285 – 295.
[6] Z. Cao, J. Engelhardt, M. Dierks, M. T. Clough, G. H. Wang, E. Heracleous, A. A. Lappas, R. Rinaldi, F. Schuth, *Angew. Chem. Int. Ed.* **2017**, *56*, 2334 – 2339; *Angew. Chem.* **2017**, *129*, 2374 – 2379.
[7] R. W. Snell, E. Combs, B. H. Shanks, *Top. Catal.* **2010**, *53*, 1248 – 1253.
[8] M. Milina, S. Mitchell, J. Pérez-Ramírez, *Catal. Today* **2014**, *235*, 176 – 183.
[9] T. N. Pham, D. Shi, D. E. Resasco, *Appl. Catal. B* **2014**, *145*, 10 – 23.
[10] H. Hernando, S. Jiménez-Sánchez, J. Fermoso, P. Pizarro, J. M. Coronado, D. P. Serrano, *Catal. Sci. Technol.* **2016**, *6*, 2829 – 2843.
[11] S. Wan, Y. Wang, *Front. Chem. Sci. Eng.* **2014**, *8*, 280 – 294.
[12] A. Galadima, O. Muraza, *Energy Convers. Manage.* **2015**, *105*, 338 – 354.
[13] T. Carlson, J. Jae, Y. Lin, G. Tompsett, G. Huber, *J. Catal.* **2010**, *270*, 110 – 124.
[14] M. Zabeti, T. S. Nguyen, L. Lefferts, H. J. Heeres, K. Seshan, *Bioresour. Technol.* **2012**, *118*, 374 – 381.
[15] M. Zabeti, J. Baltrusaitis, K. Seshan, *Catal. Today* **2016**, *269*, 156 – 165.
[16] Q. Lu, Z. Tang, Y. Zhang, X. Zhu, *Ind. Eng. Chem. Res.* **2010**, *49*, 2573 – 2580.
[17] E. H. Lee, M. J. Jeon, J. K. Jeon, D. J. Suh, S. H. Park, B. Seo, S. H. Joo, Y. K. Park, *J. Nanosci. Nanotechnol.* **2014**, *14*, 2343 – 2351.
[18] D. Fabbri, C. Torri, V. Baravelli, *J. Anal. Appl. Pyrolysis* **2007**, *80*, 24 – 29.
[19] X. Zhang, L. Sun, L. Chen, X. Xie, B. Zhao, H. Si, G. Meng, *J. Anal. Appl. Pyrolysis* **2014**, *108*, 35 – 40.
[20] S. D. Stefanidis, S. A. Karakoulia, K. G. Kalogiannis, E. F. Iliopoulou, A. Delimitis, H. Yiannoulakis, T. Zampetakis, A. A. Lappas, K. S. Triantafyllidis, *Appl. Catal. B* **2016**, *196*, 155 – 173.
[21] M. I. Nokkosmäki, E. T. Kuoppala, E. A. Leppämäki, A. O. I. Krause, *J. Anal. Appl. Pyrolysis* **2000**, *55*, 119 – 131.
[22] Y. T. Cheng, J. Jae, J. Shi, W. Fan, G. W. Huber, *Angew. Chem. Int. Ed.* **2012**, *51*, 1387 – 1390; *Angew. Chem.* **2012**, *124*, 1416 – 1419.
[23] T. C. Hoff, M. J. Holmes, J. Proano-Aviles, L. Emdadi, D. Liu, R. C. Brown, J. P. Tessonnier, *ACS Sustainable Chem. Eng.* **2017**, *5*, 8766 – 8776.
[24] A. A. Lappas, K. G. Kalogiannis, E. F. Iliopoulou, K. S. Triantafyllidis, S. D. Stefanidis, *WIREs Energy Environ.* **2012**, *1*, 285 – 297.
[25] C. Hu, R. Xiao, H. Zhang, *Bioresour. Technol.* **2017**, *243*, 1133 – 1140.
[26] J. Fermoso, H. Hernando, S. Jiménez-Sánchez, A. A. Lappas, E. Heracleous, P. Pizarro, J. M. Coronado, D. P. Serrano, *Fuel Process. Technol.* **2017**, *167*, 563 – 574.
[27] H. Hernando, J. Fermoso, I. Moreno, J. M. Coronado, D. P. Serrano, P. Pizarro, *Biomass Convers. Biorefin.* **2017**, *7*, 277 – 287.
[28] H. Hernando, I. Moreno, J. Fermoso, C. Ochoa-Hernández, P. Pizarro, J. M. Coronado, J. Čejka, D. P. Serrano, *Biomass Convers. Biorefin.* **2017**, *7*, 289 – 304.
[29] J. Fermoso, H. Hernando, P. Jana, I. Moreno, J. Přech, C. Ochoa-Hernández, P. Pizarro, J. M. Coronado, J. Čejka, D. P. Serrano, *Catal. Today* **2016**, *277*, 171 – 181.
[30] Y. T. Cheng, G. W. Huber, *Green Chem.* **2012**, *14*, 3114 – 3125.
[31] E. F. Iliopoulou, S. Stefanidis, K. Kalogiannis, A. C. Psarras, A. Delimitis, K. S. Triantafyllidis, A. A. Lappas, *Green Chem.* **2014**, *16*, 662 – 674.
[32] A. Zheng, Z. Zhao, S. Chang, Z. Huang, H. Wu, X. Wang, F. He, H. Li, *J. Mol. Catal. A* **2014**, *383 – 384*, 23 – 30.
[33] R. French, S. Czernik, *Fuel Process. Technol.* **2010**, *91*, 25 – 32.
[34] M. M. Yung, A. R. Stanton, K. Iisa, R. J. French, K. A. Orton, K. A. Magrini, *Energy Fuels* **2016**, *30*, 9471 – 9479.
[35] H. Hernando, A. M. Hernández-Giménez, C. Ochoa-Hernández, P. C. A. Bruijnincx, K. Houben, M. Baldus, P. Pizarro, J. M. Coronado, J. Fermoso, J. Čejka, B. M. Weckhuysen, D. P. Serrano, *Green Chem.* **2018**, *20*, 3499 – 3511.
[36] H. Hernando, C. Ochoa-Hernández, M. Shamzy, I. Moreno, J. Fermoso, P. Pizarro, J. M. Coronado, J. Čejka, *Catal. Sci. Technol.* **2019**, *9*, 789 – 802.
[37] J. Zhang, X. Liu, *Phys. Chem. Chem. Phys.* **2014**, *16*, 8655 – 8660.
[38] W. F. Bradley, *Mineralogist* **1940**, *25*, 405 – 410.
[39] E. L. Wu, S. L. Lawton, D. H. Olson, A. C. Rohrman, Jr., G. T. Kokotailo, *J. Phys. Chem.* **1979**, *83*, 2777 – 2781.
[40] A. G. Alvarez, H. Viturro, R. D. Bonetto, *Mater. Chem. Phys.* **1992**, *32*, 135 – 140.
[41] M. Hunger, *Solid-State NMR Spectroscopy, in Zeolite Characterization and Catalysis: A Tutorial* (Eds.: A. W. Chester, E. G. Derouane), Springer, Berlin, **2009**, pp. 65 – 105.
[42] L. Rodríguez-González, F. Hermes, M. Bertmer, E. Rodríguez-Castellón, A. Jiménez-López, U. Simon, *Appl. Catal. A* **2007**, *328*, 174 – 182.
[43] A. Samoson, E. Lippmaa, G. Engelhardt, U. Lohse, H. G. Jerschkewitz, *Chem. Phys. Lett.* **1987**, *134*, 589 – 592.
[44] S. Y. Choi, Y. S. Park, S. B. Hong, K. B. Yoon, *J. Am. Chem. Soc.* **1996**, *118*, 9377 – 9386.
[45] Z. Yan, D. Ma, J. Zhuang, X. Liu, X. Liu, X. Han, X. Bao, F. Chang, L. Xu, Z. Liu, *J. Mol. Catal. A* **2003**, *194*, 153 – 167.
[46] J. S. J. Hargreaves, A. L. Munnoch, *Catal. Sci. Technol.* **2013**, *3*, 1165 – 1171.
[47] I. L. C. Buurmans, E. A. Pidko, J. M. de Groot, E. Stavitski, R. A. van Santen, B. M. Weckhuysen, *Phys. Chem. Chem. Phys.* **2010**, *12*, 7032 – 7040.
[48] I. L. C. Buurmans, J. Ruiz-Martinez, W. V. Knowles, D. van der Beek, J. A. Bergwerff, E. T. C. Vogt, B. M. Weckhuysen, *Nat. Chem.* **2011**, *3*, 862 – 868.
[49] I. L. C. Buurmans, J. Ruiz-Martinez, S. L. van Leeuwen, D. van der Beek, J. A. Bergwerff, W. V. Knowles, E. T. C. Vogt, B. M. Weckhuysen, *Chem. Eur. J.* **2012**, *18*, 1094 – 1101.
[50] Z. Ristanović, A. V. Kubarev, J. Hofkens, M. B. J. Roeffaers, B. M. Weckhuysen, *J. Am. Chem. Soc.* **2016**, *138*, 13586 – 13596.
[51] N. Y. Chen, T. F. Degnan Jr., L. R. Koenig, *ChemTech* **1986**, *16*, 506 – 511.
[52] W. O. Haag, P. G. Rodewald, P. B. Weisz (Mobil Oil Corporation, New York, NY), US4300009, **1981**.

Manuscript received: February 22, 2019
Revised manuscript received: March 22, 2019
Accepted manuscript online: March 26, 2019
Version of record online: May 16, 2019